Sustainable Materials and Technologies 33 (2022) e00488

Contents lists available at ScienceDirect

Sustainable Materials and Technologies

journal homepage: www.elsevier.com/locate/susmat

A resource-efficient process design for heavy fabrication: A case of single-pass-per-layer narrow gap welding

Uttam Kumar Mohanty [a,1], Angshuman Kapil [b,1], Yohei Abe [c], Tetsuo Suga [d], Manabu Tanaka [d], Abhay Sharma [b,*]

[a] Indian Institute of Technology Hyderabad, Telangana, India
[b] KU Leuven, Department of Materials Engineering, Campus De Nayer, Sint-Katelijne Waver, Belgium
[c] Technical Research Institute, Hitachi Zosen Corporation, Osaka, Japan
[d] Joining & Welding Research Institute, Osaka University, Japan

ARTICLE INFO

Keywords:
Narrow gap
Submerged arc welding
Sustainability
Single-pass-per-layer
Process design
Heat-resistant steel

ABSTRACT

The welding process, omnipresent in the heavy fabrication industry, is a potential source of hazardous emissions. The article is motivated by the need to improve the sustainability of the heavy fabrication processes. Single-pass-per-layer narrow gap welding (NGW) is a potential alternative for reducing carbon footprint in high-thickness joints conventionally fabricated using the multi-pass multi-layers, sometimes even 100 or more layers, which is time-, material-, and energy- consuming. A newly developed mathematical model allows process design based on resource-efficient bead-on-plate welds (i.e., one layer deposited on a substrate). The results of bead-on-plate experiments are firstly utilized to identify the process capabilities in terms of strength, process, and production measures and subsequently coupled with the NGW mathematical model to arrive at feasible process parameters for a given groove design. The proposed approach implemented for a candidate case reveals significant improvement in the utilization of process capabilities, i.e., increase in strength, melting efficiency, and deposition rate and reduction in energy and material consumption. This investigation brings out three fundamental design rules for single-pass-per-layer NGW, namely i) the corresponding width of the bead-on-plate weld should be >1.5 times the groove width, ii) an upper limit on the utilization of process capabilities exists beyond which the productivity goes down drastically, and iii) the upper limit can be realized only at critical layer thicknesses. The design approach can be implemented to achieve more productive, economical, and sustainable design for processes involving high energy and material consumption.

1. Introduction

Driven by the increased demand for larger and heavier steel members in pressure vessels, pipelines, shipbuilding, nuclear, submarine, and other related applications, the weld assembly times, and production costs have grown manifolds [1]. Much focus has been on alleviating these issues and improving welding process economics by reducing joint completion and post-weld inspection and repair times [2]. Along these lines, several attempts have been directed towards reducing the weld size or volume of the joint [3], improving current welding processes [4], incorporating new welding techniques [5,6], and process automation [2]. Despite these efforts, there is a need to develop a framework for resource-efficient welding process design, considering energy and material efficiencies, in line with the other processes like subtractive, additive and hybrid manufacturing processes [7]. Recently, efforts have been put to conduct systematic studies with a particular focus on the energy efficiency, sustainability, and impact on the environment for various welding processes like laser welding [8,9], gas metal arc welding [10], laser-arc hybrid welding [11], friction stir welding [12], and resistance spot welding [13]. Sustainable manufacturing is a topic of global interest for both industries and researchers likewise. Efforts to improve the welding processes with the larger focus on contributing to sustainable manufacturing has been reported in literature for different welding processes like twin-wire submerged arc welding (SAW) [14],

* Corresponding author.
E-mail addresses: uttam.baleshwar@gmail.com (U.K. Mohanty), angshuman.kapil@kuleuven.be (A. Kapil), y_abe@hitachizosen.co.jp (Y. Abe), suga@jwri.osaka-u.ac.jp (T. Suga), tanaka@jwri.osaka-u.ac.jp (M. Tanaka), abhay.sharma@kuleuven.be (A. Sharma).
[1] These authors have contributed equally to this work.

https://doi.org/10.1016/j.susmat.2022.e00488
Received 22 June 2022; Received in revised form 23 August 2022; Accepted 30 August 2022
Available online 5 September 2022

and tandem gas metal arc welding (TGMAW) [15]. In addition, to evaluate the environmental effect of welding processes, an ISO standardized method, viz. Life Cycle Assessment (LCA), has been adopted for a variety of welding processes. The goal behind these studies varied from comparing the environmental impacts and the risk hazard of welders caused by welding fumes [16], environmental impact of welding training [17], direct comparison of the environmental impact of two different welding processes [18] and generating designer awareness about welding technologies (use of design documentation) [19]. LCA has also been adopted for medium thick welds ($\leq$20 mm) in order to improve the processes and equipment for more environmental friendliness [11,20].

One of the specific measures for improving welding economics (energy and material efficiencies) for thick welds that has attracted attention from industries is narrow gap welding (NGW). The NGW process employs narrow grooves, with groove widths ranging from around 8 mm (for gas tungsten arc welding) up to 20 mm (for SAW) [2]. NGW significantly reduces the weld metal volume and, correspondingly, the welding time. Achieving a considerable reduction in deposited weld metal volume requires careful consideration of the joint configuration and the design of the process. The use of narrower joint gaps and decreased preparation angles directly impacts productivity and hence the manufacturing cost. Narrow gap submerged arc welding (NG SAW), due to its high deposition rates, exceptional weld quality, and flexibility of process modifications, is suitable for narrow gap applications, particularly for welding thicker sections (>50 mm) [21,22]. Several approaches have been adapted to achieve higher deposition rates in NG SAW, including higher heat input, increased travel speed, longer wire extension length, multiple electrodes, and metal powder addition [23]. However, these approaches have numerous associated downsides that dominate the achievable advantages. An increase in heat input leads to increased dilution of base metal and slower cooling rates, leading to a coarse-grained microstructure that makes the joint brittle at lower operating temperatures. Higher travel speeds can lead to welding defects such as undercut and cracks. Although using multiple electrodes helps negate the issue of welding defects when higher travel speeds are employed, multiple electrodes increase the process complexity [23].

One of the other ways to achieve higher deposition rates in NG SAW of thick sheets is single-pass-per-layer welding. Applying the single-pass-per-layer technique reduces the cross-sectional area of the groove and, at the same time, reduces the number of passes and the consumption of filler material, thereby reducing welding time and cost. Although this process variant has existed since the advent of the NGW process [24], its usage has been limited due to the possible occurrence of lack of fusion, especially in the sidewalls, slag entrapment and difficulty of slag removal, and higher average heat input to the base metals compared to the multi-pass-per-layer modes [2]. In recent years, with the advent of advanced power sources, research has been directed towards single-pass-per-layer welding of extremely thick sheets [25,26], with the larger goal of developing the technique for industrial applications.

The literature on single-pass-per-layer NGW has been mostly directed towards the experimental determination of appropriate welding parameters to prevent defects and produce joints with acceptable mechanical properties. In contrast, very little work has been conducted on process modeling and developing process design approaches. Seminal work on single-pass-per-layer NGW by Tokuhisa et al. [27] focused on developing welding consumables for NG SAW of Cr—Mo steel. The key aspect of their study was determining the composition of the consumables that could produce homogenous and high toughness welds. Manzoli et al. [21] evaluated the NGW process economics with different process variants, including single-pass-per-layer NGW. Recent work by Fusari et al. [25] on NG SAW of Cr—Mo steel revealed that the two-beads-per-layer technique results in a localized central zone with a fine-grained structure, which is not desirable for creep resistance. To eliminate this potential critical zone, the single-pass-per-layer welding technique was developed, which leads to the production of weld joints with superior creep resistance and toughness. The concept of ultra-narrow gap SAW using the single-pass-per-layer technique was recently explored by Abe et al. [28]. A method of selecting appropriate welding conditions (based on experimental trials) that can lead to defect-free joints was proposed, followed by developing a model that could predict the occurrence of lack of fusion during bead-on-plate welding. Mathematical models that can predict optimized welding parameters for preventing sidewall fusion defects, ease slag detachment and prevent solidification cracking for single-pass-per-layer NG SAW have also been developed [29,30]. The parameters predicted by these models could produce concave weld surfaces with optimum depth-to-width ratios and maximum lateral penetration. Abe et al. [31] related the results of bead-on-plate welding with the layer thickness in single-pass-per-layer NG SAW. However, these studies are restricted to certain parameters and provide a limited understanding of the process capability and process design approach. Despite the findings and limited accumulated knowledge of the single-pass-per-layer NG SAW process, the obscure operational details merit a detailed investigation to ensure widespread applicability.

Implementation of single-pass-per-layer NGW requires the deposited weld bead to be wide enough to fill the groove and at the same time remain almost flat. To implement the technology at the workshop level, it is necessary to have a fundamental relationship between the process conditions and the obtained results, together with process design guidelines. Determination of optimized welding parameters through repeated experiments in NGW is time, cost, and resource prohibitive. The resources have an exponential increase with large-scale high thickness structures, where the weld length and weld metal to be deposited are large. To establish single-pass-per-layer NG SAW as a viable process and negate the cost and time expenses involved in NG SAW experimentation, this study presents a novel route for determining process capability through resource-efficient bead-on-plate experiments coupled with a process design approach. Currently, models do not exist in the literature for optimizing NG SAW that utilizes a single pass in each layer. The narrow gap joint with single-pass-per-layer needs each pass to produce a flat surface resembling the base plate in bead-on-plate welding. The moot point is that if the optimal conditions for multi-pass NG SAW can be obtained with bead-on-plate welds, the experimentation cost and time can be significantly reduced. This investigation is the first study where the bead-on-plate experiments are extended for NGW process design. The primary objective of this work is the realization of a design approach for the single-pass-per-layer NG SAW process, utilizing process models of penetration, bead width, bay area, dilution, melting efficiency, heat input, flux-wire ratio, deposition rate.

Fig. 1 provides an overview of the approach adopted in this study. The proposed approach is based on authors' experience on submerged arc welding [14] as well as NGW [28,31]. The idea of incorporating sustainability aspect in welding is also derived from authors experience and previous work [14].The larger goal of designing and optimizing the single-pass-per-layer NGW process using bead-on-plate experiments is achieved in sequential steps. Firstly, process models for bead-on-plate welds are developed and validated based on experimental runs. Based on the process models, the process capability is determined in terms of optimal process outcomes (maximum penetration, dilution, melting efficiency and minimum bay area) under constraints of heat input and flux-wire ratio. The process outcomes and constraints are described in detail in the succeeding sections. From the results of the bead-on-plate process models, layer-wise deposition rates are calculated and compared with the actual deposition rates in groove welding conditions. A process design approach is suggested once the applicability of bead-on-plate results for groove welding is established. The process design approach is based on a mathematical model to ensure a flat deposition in a narrow gap condition. The flat surface model (FSM) is executed on a test case of a narrow groove. Process capabilities for different layer thicknesses are identified for the maximum deposition rate, leading to feasible layer thicknesses. Detailed scheme of experiments and process

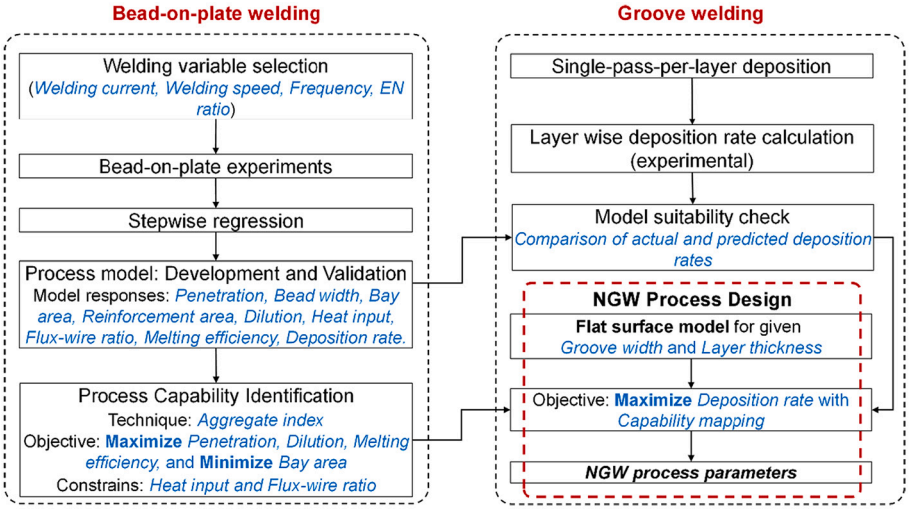

Fig. 1. Overview of the experimental and modeling approach.

modeling are presented in the succeeding sections.

The larger goal of this study is to obtain the process conditions that can yield optimum weld attributes, process and production measures for a given groove design and desired layer thickness. The specific objective is to showcase the application of the proposed model to identify process parameters that could improve the resource efficiency for a practical case of NGW in heat-resistant steel. The set of parameters fulfil the welding procedure specification (WPS) used for heavy fabrication of actual high-thickness components and thus are expected to ensure the mechanical and corrosion performance. Although the concept of sustainability has been studied for various welding processes, there is no reported literature that considered the idea of utilizing resource-efficient bead-on-plate welding for process modeling and realization of design parameters for single-pass-per-layer NGW. To the authors best knowledge this is one of the first-of-its-kind study, where a model has been developed for a practical case of NGW. Conventionally the welding processes are optimized based on maximum penetration and dilution to ensure optimal strength. The current model is augmented by incorporating process (heat input and flux-wire ratio) and production measures (melting efficiency and deposition rate). Thus, the considered subset encompasses more parameters than the existing models. Moreover, the set of parameters fulfil the WPS used for heavy fabrication of actual high-thickness components. The proposed approach is implemented on 2.25Cr-1Mo heat-resistant steel using the square alternating current (AC) waveform SAW. The experimental details below are followed by a description of how the proposed process models and process design approach are developed. The results are then discussed in the framework of process models, process capability and process design. This is followed by a detailed evaluation of the efficacy of the developed design approach in terms of the strength, process, and production measures that eventually decide the economics and efficiency of the process. Finally, the possibilities of this novel approach, together with future research directions, are pointed out.

2. Materials and method

2.1. AC square waveform SAW

The present study utilizes the AC square waveform. Conventionally, direct current (DC) power sources are used in SAW. Typically, direct current electrode positive (DCEP) polarity results in deep penetrating narrow bead, whereas direct current electrode negative (DCEN) polarity results in shallow and wide bead, as observed in Fig. 2. The application of AC allows alteration of the bead shape; however, the use of AC power

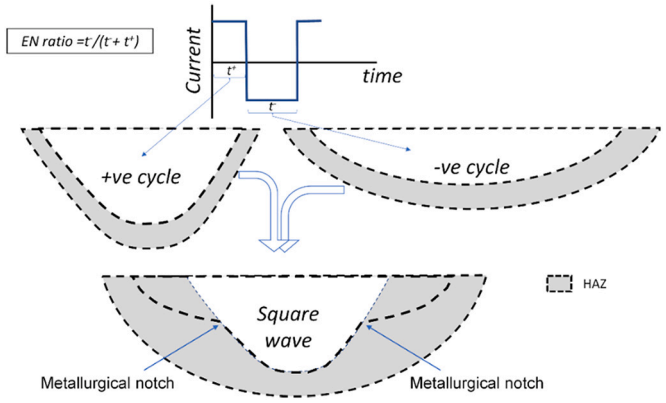

Fig. 2. AC square waveform showing current cycle, EN ratio, developed weld bead shape and the location of the metallurgical notch.

source in SAW has been limited because of the crossover problem (polarity reversal), i.e., arc extinguishing due to lower voltage when polarity reverses [32]. Due to this issue, the AC power source is used along with a DC power source in tandem welding, where two power sources are used. The polarity reversal issue has been solved by developing a power source that uses AC square characteristics (Fig. 2). The positive and negative portions of the current cycle can be controlled for their respective duration and amplitude. The fraction of the current cycle for which the electrode remains negative is known as the electrode negativity (EN) ratio. Compared to the DCEP, the AC square waveform is recommended for improved toughness in low-temperature environments, particularly for pressure vessels, and pipelines [33]. Moreover, the AC square waveform can maintain higher penetration even at higher welding speeds [32]. The square waveform also allows control of the shape of the top surface of the bead in SAW [34]. On the downside, the instantaneous reversal of polarity in square waveform causes the power source to act like two alternatively operating DCEP and DCEN sources. Consequently, the weld bead shape in the square waveform resembles two overlapping beads obtained by DCEP (deep penetrating narrow bead) and DCEN (shallow and wide bead), as observed in Fig. 2. The intersection of two overlapping beads may cause a metallurgical notch with a square waveform (Fig. 2) [35,36]. The effect of this metallurgical notch is quantified as the bay area, which needs to be controlled by selecting appropriate process parameters, as incorporated in this study. Table 1 provides a summary of the aspects of AC square waveform

Table 1
Aspects of AC square waveform.

	DCEP	DCEN	AC Square waveform
EN ratio	0	1	$0 < EN < 1$
Penetration	Deep	Shallow	Composite (Fig. 2)
Weld width	Narrow	Wide	Wide
Metallurgical notch	Absent	Absent	Present

depicted in Fig. 2.

2.2. Material, experimental parameters, and weld specimen

In this investigation, 2.25Cr-1Mo heat-resistant steel was chosen as the candidate base material. A US-521S wire of 4 mm diameter was used as the electrode material. The combination of wire and flux materials was selected as per the AWS classification (AWS A5.23 F9P2-EG-B-3) for the AC power source. The PF-200 10 × 48 mesh flow was chosen as the flux material. The chemical compositions of the electrode and the base material are provided in Table 2.

The process parameters, which act as inputs for development of models for industrial processes must be practically controllable, such that the developed models are applicable at the shop floor. Controllable process parameters available with the machine set up, namely, welding current (I), welding speed (S), current frequency (F), and EN ratio, were varied to obtain the data for developing the process models. These parameters, quantify the welding conditions, and are principally controlled during the AC square waveform SAW process [32]. Other parameters (e.g., electrode diameter, welding voltage, and contact-tip-to-work distance (CTWD)) are fixed based on the working range of the controllable parameters.

The real-time transient welding current and voltage were measured to calculate the heat input during the bead-on-plate welding experiments. The weights of the baseplate and flux were measured using a microbalance. In this investigation, four parameters, i.e., welding current (I), welding speed (S), current frequency (F), and EN ratio, were varied to obtain the data for developing the process models. The welding experiments were conducted at Hitachi-Zosen Corporation, Japan, with variations of welding current between 400 and 700 A, welding speed between 20 and 50 cm/min, current frequency between 20 and 80 Hz, and EN ratio between 0.25 and 0.75. The welding voltage and CTWD were constant at 30 V and 30 mm, respectively. For the development of the process models, the welding process parameters were normalized between 0 and 1 using Eq. (1). The normalization nullifies the differences in the dimensionality and span of the inputs.

$$x_{normalized} = \frac{x_i - x_{min}}{x_{max} - x_{min}} \tag{1}$$

where the variable x denotes the welding process parameter, x_{min} and x_{max} denote the minimum and maximum values of the corresponding welding process parameter.

Fig. 3(a) provides a schematic representation of the bead-on-plate welding setup. Fig. 3(b) depicts the design for groove welding. In this study, the groove weld deposition was used to check the applicability of the bead-on-plate process models for NGW. For steel plates below 70 mm in thickness (55 mm in this study, Fig. 3(b)), it has been reported in literature that for V-shaped grooves, a groove angle of 30^0 is optimum that enables the deposition of sound weld beads without any defects [4]. As seen in Fig. 3(b), a variable width groove with a groove angle of 30^0

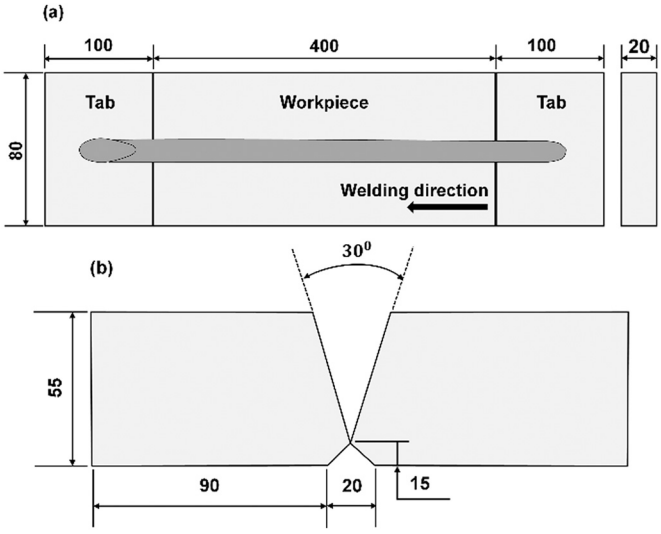

Fig. 3. (a) Schematic representation of the bead-on-plate welding set up, and (b) design of the groove joint utilized for deposition and calculation of layer-wise deposition rates (All dimensions are in mm, schematics not drawn to scale).

(bevel angle of 15^0) was chosen to deposit the layers in this study. The layer-wise deposition rates were calculated and compared with those predicted by the bead-on-plate process models. Another rationale behind selecting a varying width groove design was to check the sensitivity of the deposition rate with variation in groove width. The developed bead-on-plate process models were then utilized to design and optimize the NGW process for a particular test case of a narrow groove width of 14 mm. The 14 mm groove width (W_g) has been experimentally proven successful for NGW [28] and thus has been chosen for this study. Note that the schematic provided in Fig. 3(b) refers to the test run for measuring the deposition rate.

2.3. Scheme of the experimentation

This investigation incorporated two-stage experiments. The first stage consisted of the bead-on-plate welding experiments, whereas the second stage covered layer-wise deposition in the groove joint. Both the experimental stages were conducted using the AC square waveform power source. For bead-on-plate welding, a total of 26 experiments were conducted. The data were randomly divided into two parts of 21 and 5 experiments, each for model development and validation, respectively, as shown in Table 3. The process parameters varied in this study (welding current, welding speed, frequency, and EN ratio) are the ones that were controllable for the available welding power source and welding torch. The variation in the parameters was based on a one parameter at a time design of experiments. The range chosen for the variation is also derived from authors technical knowhow of the process and the available equipment.

The groove design (set up shown in Fig. 3(b)) followed a single-pass-per-layer deposition procedure, wherein five layers were deposited. In this study, two different deposition conditions called base deposit and high deposit (Table 4), were employed for single-pass-per-layer deposition in the groove joint. The base deposit refers to conditions currently employed in industry for the material and flux-wire combination used in

Table 2
Chemical composition of electrode and base material (wt%).

	Si	C	Mn	P	Ni	S	Cr	Mo	Cu	Fe
Electrode	0.13	0.16	0.93	0.003	0.14	0.002	2.45	1	0.12	Balance
Base material	0.14	0.13	0.5	0.007	–	0.002	2.36	0.97	–	Balance

Table 3
Experimental results of bead-on-plate welding.

	Process parameters					Strength measures (Bead attributes)					Process measures		Production measures	
	Exp No.	I (A)	S (cm/min)	F (Hz)	EN ratio	P (mm)	W (mm)	A_b (mm^2)	A_r (mm^2)	D (%)	HI (kJ/mm)	FWR	η_m (%)	DR (g/min)
	1	500	30	60	0.5	4.2	24.2	26.5	44.3	53.2	3.1	1.4	59.1	99.0
	2	700	30	60	0.5	7.6	27.2	70.9	81.4	54.7	4.4	0.8	80.4	166.5
	3	400	30	60	0.5	3.5	19.6	17.9	36.4	48.4	2.5	1.3	54.8	72.0
	4	600	30	60	0.5	5.9	26.4	51.5	59.3	55.6	3.8	1.0	69.0	129.0
	5	500	50	60	0.5	5.3	16.4	27.7	22.8	66.6	1.9	0.8	71.1	87.5
	6	500	30	60	0.75	4.2	22.6	28.5	50.7	48.3	3.1	0.9	62.8	114.0
	7	500	30	20	0.5	4.5	24.9	33.6	53.2	50.7	3.1	0.9	66.9	112.5
	8	500	30	80	0.5	4.8	25.4	38.8	44.9	49.5	3.1	1.1	61.2	102.0
	9	500	20	20	0.25	4.9	29.0	46.9	49.5	48.5	4.7	1.4	56.6	96.0
	10	500	40	40	0.4	5.4	19.8	38.1	32.6	61.6	2.4	1.2	69.9	96.0
Model development	11	500	50	80	0.75	5.4	19.2	37.2	30.9	55.7	1.9	0.9	73.7	112.5
	12	700	30	40	0.25	8.9	31.8	95.8	75.3	60.3	4.4	0.8	82.0	156.0
	13	700	20	80	0.5	8.5	33.3	110.6	128.1	47.8	6.7	0.7	71.8	177.0
	14	700	40	60	0.75	6.7	23.8	56.7	64.7	57.1	3.3	0.6	91.4	164.0
	15	700	50	20	0.4	8.3	20.2	55.4	43.7	64.4	2.6	0.6	90.9	147.5
	16	400	30	80	0.4	3.9	20.0	27.4	35.7	53.4	2.5	1.4	59.8	66.0
	17	400	50	60	0.25	4.0	14.2	16.6	22.1	58.7	1.5	1.0	68.5	70.0
	18	600	30	20	0.75	6.1	26.2	56.8	75.3	50.0	3.8	0.8	78.2	151.5
	19	600	20	60	0.4	6.6	32.4	82.4	98.6	50.8	5.6	1.1	68.9	133.0
	20	600	40	80	0.25	7.9	23.0	62.5	46.2	62.8	2.8	0.8	83.8	116.0
	21	600	50	40	0.5	5.8	19.0	39.4	35.6	63.5	2.3	1.0	84.1	127.5
	22	500	20	60	0.5	4.9	30.6	57.3	79.1	52.9	4.7	1.1	69.9	105.0
	23	500	40	60	0.5	5.0	19.6	28.3	34.5	61.5	2.3	1.3	74.5	100.0
Model validation	24	500	30	60	0.4	4.6	24.4	36.1	47.9	53.5	3.1	1.0	63.5	103.5
	25	500	30	60	0.25	5.1	27.0	42.0	44.4	55.6	3.1	1.4	61.8	88.5
	26	500	30	40	0.5	4.7	24.8	38.8	71.0	52.5	3.1	1.0	58.9	106.5

P-Penetration; W-Bead width; A_b-Bay area; A_r-Reinforcement area; D-Dilution; HI-Heat input; FWR-Flux-wire ratio; η_m-Melting efficiency; DR-Deposition rate.

Table 4
Experimental conditions for deposition in groove joint.

Deposition condition	Layer no.	I (A)	S (cm/min)	F (Hz)	EN ratio
	1	450	27	60	0.5
	2	500	30	60	0.5
Base deposit	3	600	30	60	0.5
	4	600	30	60	0.5
	5	600	30	60	0.5
	1	450	27	60	0.5
	2	500	30	60	0.5
High deposit	3	700	33	20	0.75
	4	700	33	20	0.75
	5	700	33	20	0.75

this study. High deposit is achieved by deposition at higher current settings, with an aim to ensure the robustness of the process model over a wide range of applications.

2.4. Measurement of responses

(i) **Strength measures (Bead attributes):** The samples were polished and etched with 5% Nital solution (5 ml HNO_3 + 95 ml CH_3OH) to obtain the weld macrograph, as shown in Fig. 4(a). The macrograph highlights different geometric attributes, viz., penetration (P), bay area (A_b), reinforcement area (A_r), and penetration area (A_P), as depicted schematically in Fig. 4(b). The combination of reinforcement area (A_r), and penetration area (A_P) gives the area of fusion. The bay area is a metallurgical notch due to a change in the shape of the fusion boundary, which is observed with an AC square waveform [35,36], as shown in Fig. 4 (a). The geometric attributes of the bead were measured from the weld macrograph using macros in image analysis software ImageJ. The measured weld bead attributes were then utilized to calculate the weld metal dilution (D). The expression for calculating % Dilution is given by Eq. (2):

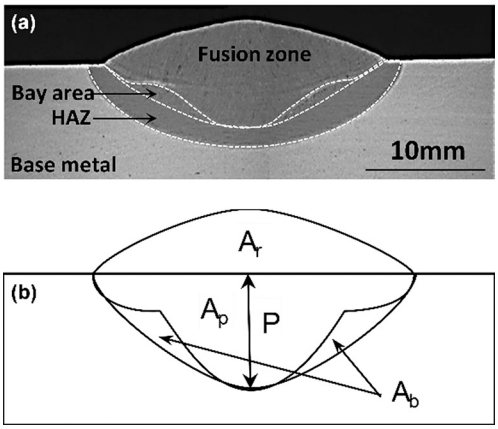

Fig. 4. (a) Macrograph showing weld cross-section produced by AC square waveform, and (b) schematic representation of the weld bead characteristics.

$$Dilution, \%D = \frac{A_p}{A_r + A_p} \times 100\% \tag{2}$$

(ii) **Process measures (Heat input and Flux-wire ratio):** The heat input was obtained by capturing the real-time transient welding current and voltage signals through the data acquisition system. If the variation in current and voltage is acquired every Δt time for n number of intervals, then heat input (HI) can be calculated using the relation (Eq.3):

$$HI = \frac{\eta \sum V_a I_a \Delta t}{nS\Delta t} = \frac{\eta \sum V_a I_a}{nS}, \frac{J}{mm} \tag{3}$$

where V_a and I_a are the actual instantaneous voltage and current in Volt

and A, respectively, η is the arc efficiency, n is the number of intervals, and S is the welding speed. The flux consumption rate to deposition rate ratio is known as the flux-wire ratio. The flux consumption rate is calculated by weighing the flux before the welding and the recovered flux. The deposition rate is measured by weighing the baseplate before and after welding. Note that, although the flux-wire ratio is a process measure, it cannot be directly controlled. A minimum flux-wire ratio = 0.6 is to be maintained to ensure the shielding of the molten metal. Flux-wire ratio of >1.2 is unwarranted because of the loss of productivity and quality [37].

(iii) **Production measures (Melting efficiency and Deposition rate):** The melting efficiency indicates the amount of material melted in the electrode and the baseplate. Therefore, melting efficiency combines both electrode and plate melting efficiency and can be expressed in terms of the penetration area (A_p), reinforcement area (A_r) and the theoretical cross-sectional area (A_{th}) as follows:

$$Plate\ melting\ efficiency, \eta_p = \frac{A_p}{A_{th}} \times 100\% \tag{4}$$

$$Electrode\ melting\ efficiency, \eta_e = \frac{A_r}{A_{th}} \times 100\% \tag{5}$$

Therefore, the total melting efficiency can be expressed as:

$$\eta_m = \eta_p + \eta_e \tag{6}$$

The theoretical cross-sectional area is calculated as per the following relation [38]:

$$A_{th} = \frac{\hat{v}}{q_{eq}} \times H_a, mm^2 \tag{7}$$

where $\hat{v}$ is the specific volume of weld metal in mm^3/g, q_{eq} is the heat required to melt a unit mass of metal, and H_a is the heat input per unit length in J/mm. The q_{eq} for AC square waveform welding of 2.25Cr-1Mo heat-resistant steel is obtained from the literature [32].

For single-pass-per-layer groove welding, the deposition rate was measured from the cross-sectional area of the deposited weld metal using the macrograph presented in Fig. 5. The following expression gives the deposition rate:

$$DR_{groove} = \frac{A_d}{n_p} S\rho, \frac{g}{min} \tag{8}$$

where A_d is the deposited area, which is the difference between the total groove area and the areas of the bottom two layers, S is the welding speed in cm/min, n_p is the number of layers, and ρ is the density of the electrode wire in g/mm^3. The measured values of the deposition rate for the base and high deposit conditions are 134.66 and 178.35 g/min, respectively.

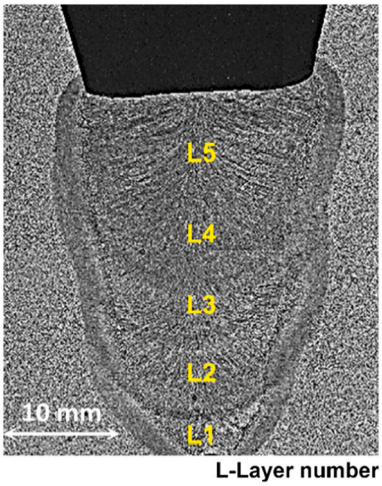

Fig. 5. Macrograph depicting the deposited layers in a typical single-pass-per-layer groove welding.

3. Process design approach

Fig. 6 provides a flowchart depicting the entire process design approach, starting with development of process models, followed by identification of process capabilities, process optimization, and eventual realization of design parameters for single-pass-per-layer NGW. Detailed explanation of the involved steps depicted in Fig. 6 is provided in Sections 3.1 to 3.4.

3.1. Process models

The responses from bead-on-plate welding experiments, i.e., the bead attributes (penetration, bead width, bay area, reinforcement area, % Dilution), process measures (heat input and flux-wire ratio), and production measures (melting efficiency and deposition rate), are used to determine the process capability. The welding speed, welding current, current frequency, and EN ratio are used as the variables to build the mathematical relations for the process models using stepwise regression with a value of α=0.15 and a confidence interval of 95%. A detailed description of the stepwise regression method employed in this work can be found in [39]. Once the applicability of bead-on-plate welding results for groove welding is established by comparing deposition rates predicted from the bead-on-plate process model with actual deposition rate in groove welding, a process design study is conducted for a test case of NGW (Fig. 1).

3.2. Process capability

The processing capability is an aggregation of different responses such as bead attributes, process measures, and production measures. The responses are chosen to have a rationale behind their selection to fulfil the requirement of the product specification and the practical requirement of higher productivity. Maximizing the bead attributes, viz., penetration and dilution, increase the weld strength. There is, however, a need to minimize the bay area. As seen in Fig. 4(a), the bay area is a distinctive feature of AC square waveform SAW and should be as minimum as possible to prevent the metallurgical notch created at the bay point. This metallurgical notch can severely degrade the mechanical properties of the weld and simultaneously act as a source of failure. The melting efficiency and deposition rates must be maximized based on production requirements. Higher melting efficiencies allow effective use of the heat (higher deposition rates) as well as positively regulates the consumption of flux in SAW. Maximizing the melting efficiency by optimizing the process parameters reduces the flux-wire ratio. The process measures, i.e., the heat input and flux-wire ratio, are the constraints to identify the process capability. The selection of heat input and flux-wire ratio as constraints help in assessing the quality and productivity of welding procedures. An increase of heat input beyond a certain value has a negative influence on the plate melting efficiency (η_p), that leads to the accumulation of molten metal under the arc, which obstructs penetration of the arc. Flux-wire ratio gives a quantitative idea of the flux consumption and a qualitative idea of the weld quality, which collectively reflect upon the productivity. A lower flux-wire ratio (<0.6) leads to contamination of the weld metal with un-melted flux and other gaseous substances. A higher flux-wire ratio (>1.2) leads to rupture of the flux cavity and subsequent flow of the molten flux. Also, with higher flux melting, the presence of a thick molten flux can cause gas entrapment.

The process capabilities are dependent on the collective effort of different features, and in particular for welding processes, the number of

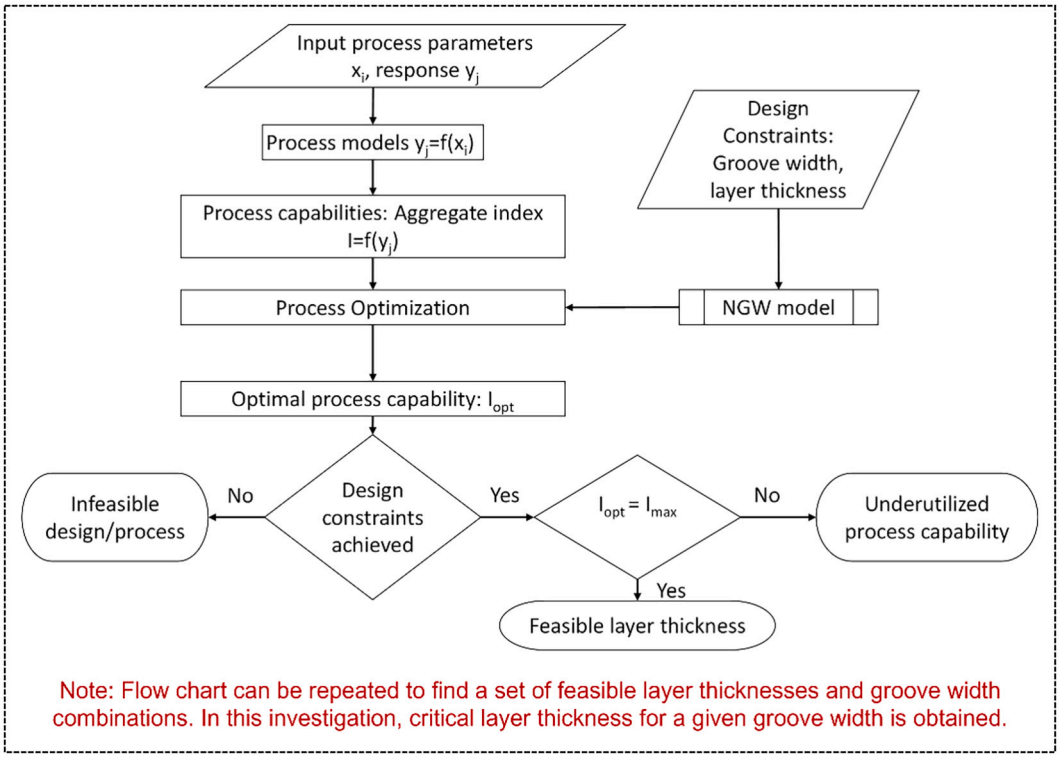

Fig. 6. Flowchart depicting the process design approach utilized in this study.

contributing features is large. As such, separate analysis of each contributing feature is cumbersome. The process capabilities in this study have been assessed by using a scheme that quantifies the collective contribution of multiple responses i.e., aggregation. The aggregation of the responses converts multiple responses into a single response. The aggregate index, suggested by Swamee and Tyagi [40] and used in this study, is as follows:

$$I_{i,n} = \left(1 - n + n\sum_{j=1}^{n} w_i S_{ij}^{-\frac{1}{k}}\right)^{-k} \tag{9}$$

where n is the number of responses, w_i is the weight, k is a constant. An optimum value of $k = 0.4$ avoids insensitiveness issues [40]. S_{ij} is the sub-index, which is a response normalized between 0 and 1. The normalization leads to indexing of the responses into the same scale. The responses in this investigation are 'smaller-the-better' or 'higher-the-better', for which sub-indices are obtained from Eqs. (10) and (11). Higher value of the normalized data symbolizes the goodness of effect of the response, i.e., 1 symbolizes the best, whereas a value of 0 symbolizes the worst.

$$\text{Smaller} - \text{the} - \text{better}\ S_{ij} = \frac{\left(Y_i^{max}\right)_j - \mathrm{Y}_{ij}}{\left(Y_i^{max}\right)_j - \left(Y_i^{min}\right)_j} \tag{10}$$

$$\text{Higher} - \text{the} - \text{better}\ S_{ij} = \frac{Y_{ij} - \left(Y_i^{min}\right)_j}{\left(Y_i^{max}\right)_j - \left(Y_i^{min}\right)_j} \tag{11}$$

where Y_{ij} is i^{th} observation for the j^{th} response, max and min represent the maximum and minimum values of the corresponding response in the considered range of experimental process parameters.

The weights for different responses in Eq. (9) are considered equal and obtained as follows:

$$w_i = \frac{1}{n} \tag{12}$$

For the evaluation of process capabilities, the objective is to obtain the maximum value of penetration, percentage dilution, melting efficiency, and the minimum value of the bay area, i.e., the number of responses (n) is equal to 4. For $n = 4$ the aggregate index is provided by Eq. (14). The sub-indices obtained from Eqs. (10) and (11) can then be applied to Eqs. (13, 14) for calculation of aggregate index for a provided set of process parameters.

$$I_{i,4} = \left(1 - 4 + 4\sum_{j=1}^{4} w_i S_{ij}^{-\frac{1}{0.4}}\right)^{-0.4} \tag{13}$$

$$\Rightarrow I_{i,4} = \left(-3 + 4\sum_{j=1}^{4} w_i S_{ij}^{-2.5}\right)^{-0.4} \tag{14}$$

3.3. Flat surface model for narrow groove deposition

The premise of the FSM is that the volume of the molten metal obtained through bead-on-plate deposition would fill the narrow groove

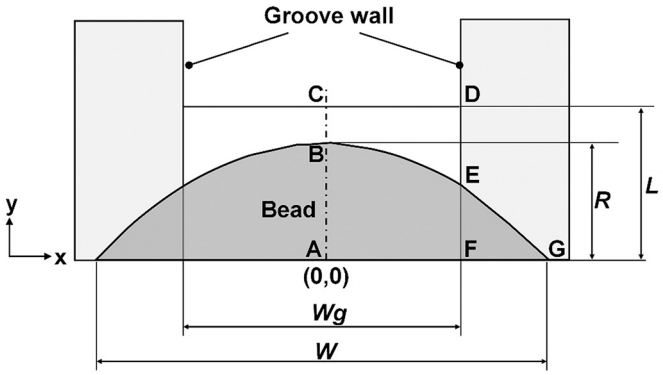

Fig. 7. Schematic representation of deposition in the narrow groove.

width (W_g) with a layer thickness (L), as shown in Fig. 7. The equivalence of bead-on-plate volume and the narrow groove volume is experimentally established and depicted in a later section. The set of process parameters in the bead-on-plate condition achieves a bead width (W) and the reinforcement height (R).

The FSM considers certain assumptions: (a) the deposited volume of the bead and the groove should be identical from the volume conservation point of view, (b) there is no lack of fusion post deposition, (c) the fluidity and surface tension of the deposited material is high enough to fill the groove width completely and form a flat top surface, and (d) the interfacial force of liquid metal and arc pressure are neglected. Following these assumptions, for a unit length, it can be deduced from Fig. 7 that:

$$Area\ (ACDF) - Area\ (ABEF) = Area\ (FEG) \tag{15}$$

$$\Rightarrow \frac{LW_g}{2} - \int_0^{\frac{W_g}{2}} R\left(1 - \frac{4x^2}{W^2}\right)dx = \int_{\frac{W_g}{2}}^{\frac{W}{2}} R\left(1 - \frac{4x^2}{W^2}\right)dx \tag{16}$$

where $\int R\left(1 - \frac{4x^2}{W^2}\right)$ is the area of the bead, considering the bead profile resembles a parabola, and x is the bead width direction.

From Eq. (16)

$$\frac{LW_g}{2} = \int_0^{\frac{W_g}{2}} R\left(1 - \frac{4x^2}{W^2}\right)dx + \int_{\frac{W_g}{2}}^{\frac{W}{2}} R\left(1 - \frac{4x^2}{W^2}\right)dx \tag{17}$$

$$\Rightarrow \frac{LW_g}{2} = \int_0^{\frac{W}{2}} R\left(1 - \frac{4x^2}{W^2}\right)dx \tag{18}$$

$$\Rightarrow \frac{LW_g}{2} = R\left(\int_0^{\frac{W}{2}} dx - \int_0^{\frac{W}{2}} \frac{4x^2}{W^2}dx\right) \tag{19}$$

$$\Rightarrow \frac{LW_g}{2} = R\left(\frac{W}{2} - \frac{4W^3}{24W^2}\right) \tag{20}$$

$$\Rightarrow LW_g = \frac{2}{3}RW \tag{21}$$

$$\Rightarrow \frac{3W_g}{2W} = \frac{R}{L} \tag{22}$$

As $R \leq L$, which leads to

$$\frac{W_g}{2} \leq \frac{W}{3} \tag{23}$$

$$\Rightarrow W \geq \frac{3}{2}W_g \tag{24}$$

From Eq. (21), the left-hand terms L and W_g are the design parameters specific to a joint, while the right-hand side terms R and W depend on the process conditions. Therefore, the design parameters must be achieved through control of bead width and reinforcement height.

3.4. Realization of design parameters

Careful selection of process parameters is necessary to achieve the process design parameters and subsequently develop process guidelines. Proper selection of process parameters leads to deposition of the required amount of material that eventually results in a flat surface without defects, as depicted in Fig. 8(a). Deposition of excess material leads to a convex top surface, resulting in slag entrapment [27] (Fig. 8(b) and (c)). In addition, violation of the flat surface condition (Eq. 24) is likely to produce a lack of fusion [28] (Fig. 8(c)).

The welds must be deposited at the maximum achievable deposition rate and the best possible utilization of process capabilities i.e., aggregate index. However, a balance between the deposition rate and aggregate index is essential, as the maximization could be detrimental to the other or make the realization of the joint infeasible. As a result, the realization of design parameters comes down to determining the mutual variation of aggregate index and deposition rate. The flat surface condition (Eq. 24) is satisfied for a given groove width and layer thickness. As a test case, design parameters $W_g = 14\ mm$ (i.e., $W \geq 21\ mm$) and $L = 2\ mm$ (i.e., $A_r = 28\ mm^2$) are realized, as explained in the next section. Subsequently, a process guideline is proposed based on varying layer thicknesses for a given groove width and the corresponding deposition rate and aggregate index.

4. Results and discussion

4.1. Process models: Development, validation, and suitability check

In this study, the correlation between the process parameters (welding current (I), welding speed (S), current frequency (F), and EN ratio) and the responses (bead attributes, process measures, and production measures) was established using a second-order polynomial. The general form of the equation, considering a constant term, can be written as:

$$Y = \sum b_i X_i + \sum b_{ii} X_i^2 + \sum b_{ij} X_i X_j + C \tag{25}$$

where Y represents the responses (penetration (P), width (W), bay area

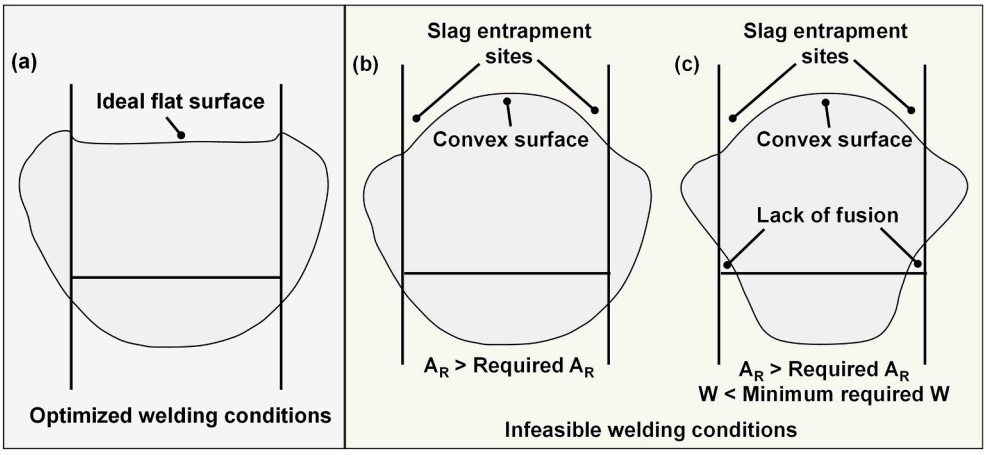

Fig. 8. Deposition in the narrow groove at (a) optimized welding conditions leading to a flat top surface, and (b) and (c) infeasible welding conditions leading to various defects.

(A_b), reinforcement area (A_r), dilution (D), heat input (HI), flux-wire ratio (FWR), melting efficiency (η_m), deposition rate (DR)), X_i, X_j are the input process parameters, b_i, b_j, and b_{ij} are the coefficients of the 1st order, 2nd order and interaction terms, respectively, and C is a constant. The values of the coefficients are obtained using the stepwise regression method described earlier. The model equations for the various responses are provided in Eqs. (26–34).

a) **Regression models for strength measures (bead attributes)**

$$P = 3.001 - 1.948\,F - 0.23\,E + 6.265\,I + 1.431\,S + 2.276\,F^2 - 1.94 - 1.782\,IS \quad (26)$$

$$W = 22.84 + 2.33\,F - 5.04\,E + 21.97\,I - 10.67\,S - 6.63\,I^2 - 5.12\,FI + 7.02\,ES - 8.15\,IS \quad (27)$$

$$A_b = -12.6\,F + 1.5\,E + 124.9\,I + 15.96\,S + 30.6\,F^2 - 25\,FI - 23.9\,EI - 76.5\,IS \quad (28)$$

$$A_r = 39.93 + 18.96\,F + 33.05\,E + 39.4\,I - 85.4\,S + 27.3\,I^2 + 56.4\,S^2 - 35.8\,FE - 46.4\,IS \quad (29)$$

$$\%D = 45.78 + 8.89\,F - 7.63\,E + 14.78\,I + 14.72\,S - 8.44\,F^2 - 8.49\,I^2 \quad (30)$$

b) **Regression models for process measures**

$$HI = 3.899 + 0.0687\,F - 0.043\,E + 2.542\,I - 5.42\,S + 3.028\,S^2 - 1.441\,IS \quad (31)$$

$$FWR = 1.688 + 0.51\,F - 0.442\,E - 0.859\,I - 0.833\,S - 0.483\,F^2 + 0.52\,ES + 0.58\,IS \quad (32)$$

c) **Regression models for production measures**

$$\eta_m = 51.77 + 9.97\,F - 6.19\,E + 14.71\,I + 10.42\,S + 11.89\,E^2 + 9.86\,I^2 - 25.9\,FE + 16.09\,ES \quad (33)$$

$$DR = 65.3 - 28.19\,F + 23.84\,E + 95.5\,I + 11.9\,S + 19.67\,F^2 + 13.28\,I^2 - 44.75\,IS \quad (34)$$

The models are functions of linear, quadratic, or interaction terms of process parameters. Most of the process models have welding current as a quadratic term, showing the welding current's significance in influencing the process. Other process parameters primarily appear as linear or interaction terms. The fit and accuracy of the models are evaluated through ANOVA and comparison of actual and predicted data in Table 5 and Fig. 9, respectively. As the average percentage prediction error in the response is significantly less, the models are good fits. The p-value (representing the probability of a null hypothesis) approaches zero, whereas the coefficient of determination (R^2) remains close to 100% for nearly all the responses in this study. This confirms that the developed process models can understand the relationship between the welding process parameters and the corresponding outputs and thus accurately predict unknown data. In Fig. 9, it can be observed that the predicted values agree with the measured values for the data used to develop and validate the model. Plots depicting variation of the attributes (Eq. 26 to 34) with process parameters are provided in Appendix (Fig. A1(a)-(i)).

The suitability of the bead-on-plate welding process models for single-pass-per-layer groove welding was then checked. For this purpose, the actual deposition rate of groove welding was measured from the cross-sectional area in both the base and high deposit conditions and compared with the predicted deposition rate (bead-on-plate process model Eq. (34) as mentioned previously. In both base and high deposit conditions, the mean absolute percentage error in the prediction of deposition rate does not exceed 3%, which indicates that the process models of bead-on-plate are suitable for groove welding application. Once validated for their accuracy, the models are used to conduct a process capability study and design the narrow gap process.

4.2. Process capability and process design

Identifying feasible working space (process capability) for bead-on-plate welds provides two-fold benefits, i.e., effective utilization of energy and resources (i.e., the welding consumables). This contributes

Table 5
Model validation results from ANOVA.

Responses		Regression			Residual error terms			Model features		
		SS	DF	MS	SS	DF	MS	F-ratio	P	R^2 (%)
Bead attributes	P	51.95	7	7.42	1.69	13	0.13	56.90	0.00	96.84
	W	525.97	8	65.74	10.06	12	0.83	78.44	0.00	98.12
	A_b	61,483.8	8	7685.5	642.7	13	49.4	155.46	0.00	98.97
	A_r	13,325.7	8	1665.72	296.1	12	24.67	67.52	0.00	97.83
	%D	651.24	6	108.54	71.42	14	5.101	21.28	0.00	90.12
Process measures	HI	32.78	6	5.46	0.12	14	0.009	610.37	0.00	99.62
	FWR	1.12	7	0.16	0.16	13	0.013	12.87	0.00	87.39
Production measures	η_m	2280.95	8	285.12	58.45	12	4.87	58.54	0.00	97.50
	DR	21,339.3	7	3048.47	187.9	13	14.45	210.93	0.00	99.13

SS-Sum square; DF-Degrees of freedom; MS-Mean square; F-ratio-Fissure ratio; P-p-value

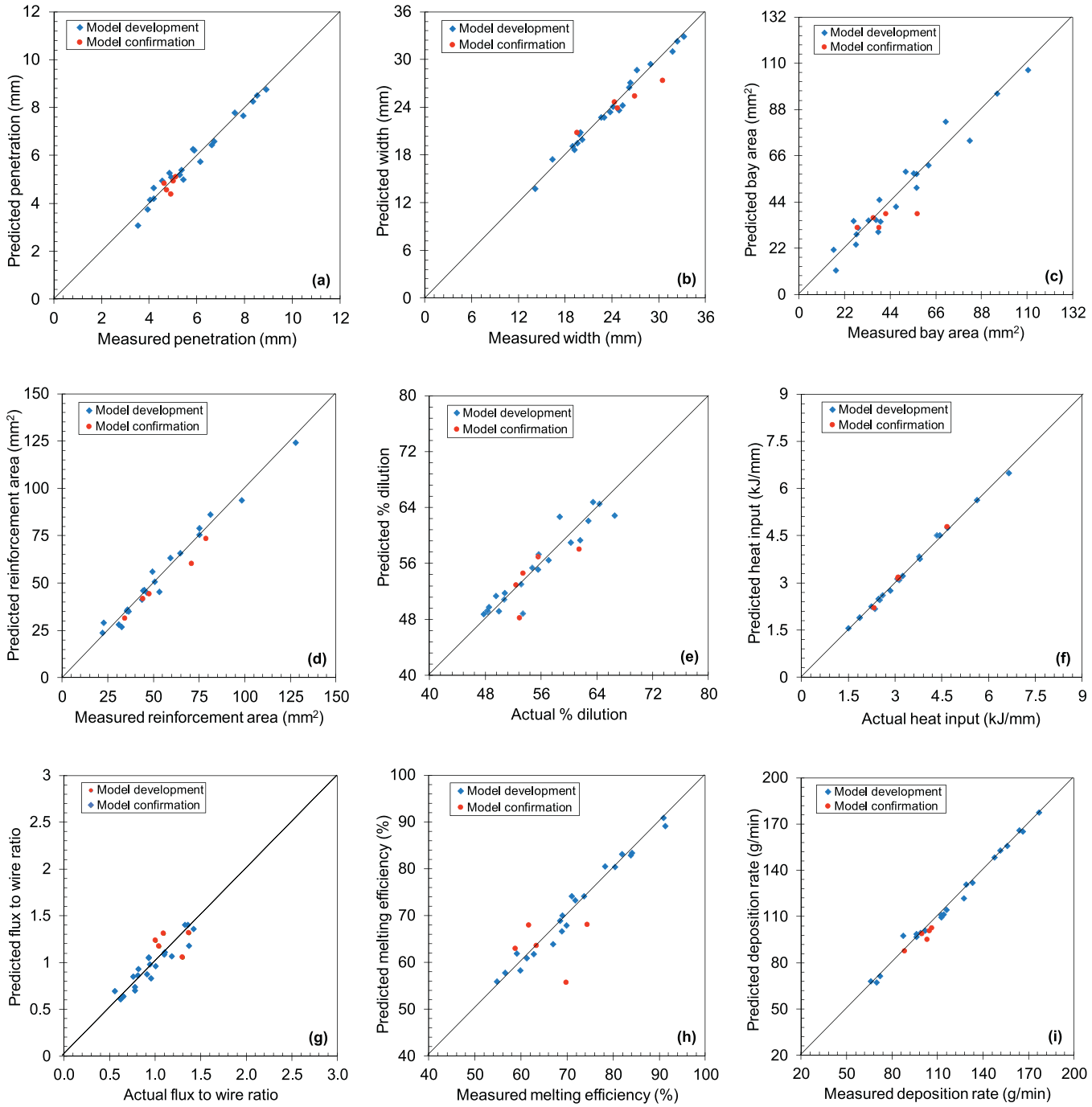

Fig. 9. Comparison between predicted and measured values of (a) penetration, (b) bead width, (c) bay area, (d) reinforcement area, (e) % dilution, (f) heat input, (g) flux-wire ratio, (h) melting efficiency, and (i) deposition rate.

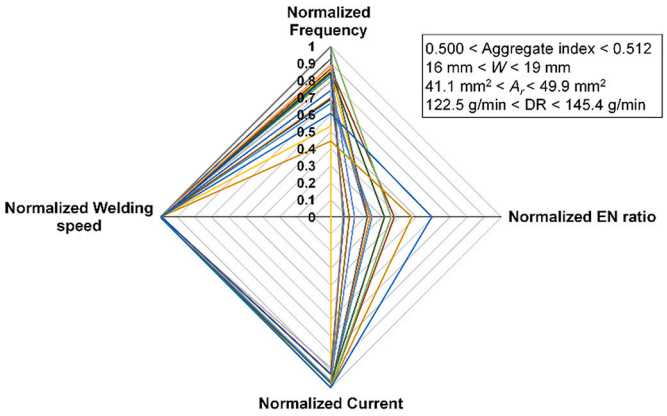

Fig. 10. Combination of normalized welding process parameters fulfilling the theoretical requirements of maximum penetration, percentage dilution, melting efficiency and the minimum bay area for bead-on-plate welding for aggregate index range between 0.5 and 0.512.

towards improving the process sustainability, which has practical implications in shop-floor conditions. The feasible working space for bead-on-plate welds further acts as an input for developing the design approach for single-pass-per-layer NG SAW.

The capability of the process was first identified, or in other words, the process was optimized using the generalized reduced gradient method to achieve maximum aggregate index (Eq. 14). The convergence value was set as 10^{-4}, and the population size considered was 100. These numbers are based on authors previous modeling work [32,36].This optimization is related to theoretical requirements of maximum penetration, percentage dilution, melting efficiency and minimum bay area and is subject to heat input and flux-wire ratio constraints, as mentioned earlier. The maximum aggregate index within the range of the selected welding process parameters was obtained to be 0.512 in this study. The corresponding maximum deposition rate was obtained as 145.4 g/min. The optimization of any actual process results in several optimal or near-optimal solutions that are practically as good as mathematically obtained unique set (if possible, to achieve); for example, Fig. 10 depicts the combination of normalized welding process parameters for aggregate index ranging between 0.5 and 0.512. It is apparent that higher operating values of welding current and welding speed can help maximize the aggregate index compared to the current frequency and EN ratio. The process is more sensitive towards the change in welding current and welding speed compared to the current frequency and EN ratio, i.e., a slight change in current and speed would alter the aggregate index, while the same would not be with the current frequency and EN ratio. The higher sensitivity of the process with change in welding current and welding speed compared to the current frequency, and EN ratio is clearly observed in Fig. A1(a) to (i), where the variation of each measured attribute with the process parameters is depicted.

For the successful implementation of single-pass-per-layer NGW, each deposited layer must fulfil the requirements of two bead attributes, i.e., reinforcement area ($A_r = 28\ mm^2$) and bead width ($W \geq 21\ mm$) for the chosen test case as explained in Sections 3.3 and 3.4. These additional requirements limit the feasible operating space for NGW. An important outcome inferred from Fig. 10 is that achieving the maximum aggregate index for bead-on-plate welding does not inherently imply successful single-pass-per-layer NGW. In the entire range of aggregate index (0.5 to 0.512), the bead width remained below the minimum requirement of 21 mm. This suggests that although the maximization of the aggregate index for bead-on-plate welding can be achieved by fulfilling the theoretical requirements of maximum penetration, percentage dilution, melting efficiency and minimum bay area, the actual production requirements for single-pass-per-layer NGW can only be accomplished by relaxing the theoretical requirements, or in other words at aggregate index values lower than the maximum achievable.

In an actual production scenario, i.e., single-pass-per-layer NGW, the definite goal is to achieve the highest deposition rate whilst being subjected to both the process constraints (heat input and flux-wire ratio) and production constraints (bead width and reinforcement area). For the case of NGW, the optimization exercise was repeated to maximize the deposition rate, i.e., the production measure, under both the process and production constraints. Fig. 11 shows the variation of the achievable deposition rates and the corresponding changes in the aggregate index, bead width and reinforcement area for the test case of NGW, with a groove width of 14 mm. Note that Fig. 11 encompasses all the attributes. The aggregate index plotted in X-axis itself takes into consideration penetration, dilution, bay area, melting efficiency, heat input, and flux-wire ratio. The rest of the attributes i.e., weld width, reinforcement area and deposition rate are plotted in the Y-axis. In line with results observed from bead-on-plate welding optimization, it can be seen in Fig. 11 that the deposition rate decreases beyond a certain aggregate index value. For the considered test case of NGW, it can be observed from Fig. 11 that there is a clear demarcation of regions wherein the NGW process is feasible or not. For aggregate index values above ~0.420, the process is infeasible as the production constraints ($W \geq 21\ mm$ and $A_r = 28\ mm^2$) are not satisfied, leading to fluctuations in the deposition rate. In the infeasible region, the bead width goes below the

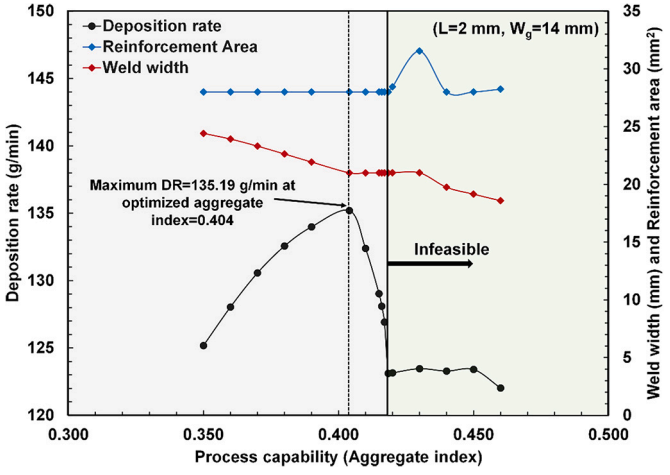

Fig. 11. Variation of achievable deposition rate, bead width and reinforcement area with the aggregate index for a test case of NGW (layer thickness = 2 mm, groove width = 14 mm).

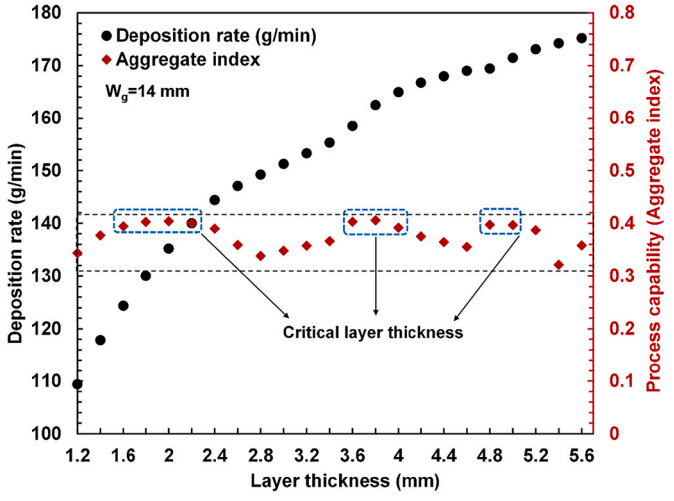

Fig. 12. Variation of deposition rate and aggregate index with layer thickness for NGW with a groove width of 14 mm.

Table 6
Variation of process capability and deposition rate with deposition types for single-pass-per-layer NGW. The process parameters corresponding to each deposition type is also provided.

Deposition type	Process capability (Aggregate Index)	Deposition rate (g/min)	Process Parameters			
			I (A)	*S* (cm/min)	*F* (Hz)	EN ratio
1-Parameters currently existing in industries	0.300	130.1	600	30	60	0.5
2-Parameters optimized to maximize deposition rate	0.404	135.1	665	47	20	0.25
3-Parameters optimized to maximize aggregate index	0.420	123.1	634	46	32.5	0.25

minimum requirement of 21 mm, which correspondingly leads to a sharp increase in reinforcement area (beyond the requirement of 28 mm^2). This type of deposition produces a surface that deviates from the ideal and desired flat surface, which is detrimental and makes the joint susceptible to various defects (Fig. 8).

The feasible region identified for the test case of NGW can be divided into two distinct regions based on the combination of process parameters employed and the aggregate index achieved. For aggregate index values lower than 0.404, although both production requirements of bead width and reinforcement area are satisfied, the deposition rates are lower than the maximum achievable. In the feasible region and for aggregate index values above 0.404, although both bead width and reinforcement area requirements are satisfied, the same comes at a drastic reduction in the deposition rate. It is clear that, for NGW, there is a unique set of process parameters that simultaneously maximize the deposition rate and satisfy both the process and production constraints. In this study, an optimum aggregate index of 0.404 produced the highest achievable deposition rate of 135.19 g/min under fully constrained conditions for single-pass-per-layer NGW.

In practice, the end-user can work with different layer thicknesses, which can impact the process capability and the deposition rate. The optimization exercise and thereafter results presented in Fig. 11 were thus repeated for a range of layer thicknesses on the narrow groove. The groove width was kept constant at 14 mm, such that the minimum width requirement for all the layer thickness values remains as $W \geq 21\ mm$ (Eq. 24). The minimum requirement of reinforcement area varies with each layer thickness. Note that for the considered range of welding parameters, the groove width (and the corresponding bead attribute requirements), the feasible layer thicknesses are between 1.2 and 5.6 mm. Fig. 12 presents the variation of optimized aggregate index values and corresponding maximum achievable deposition rates for different layer thicknesses in the feasible range. It is seen that with an increase in layer thickness, the deposition rate continuously increases; however, the aggregate index values fluctuate (between ~0.3 to 0.4). The fluctuations in aggregate index with the variation of layer thickness can be attributed

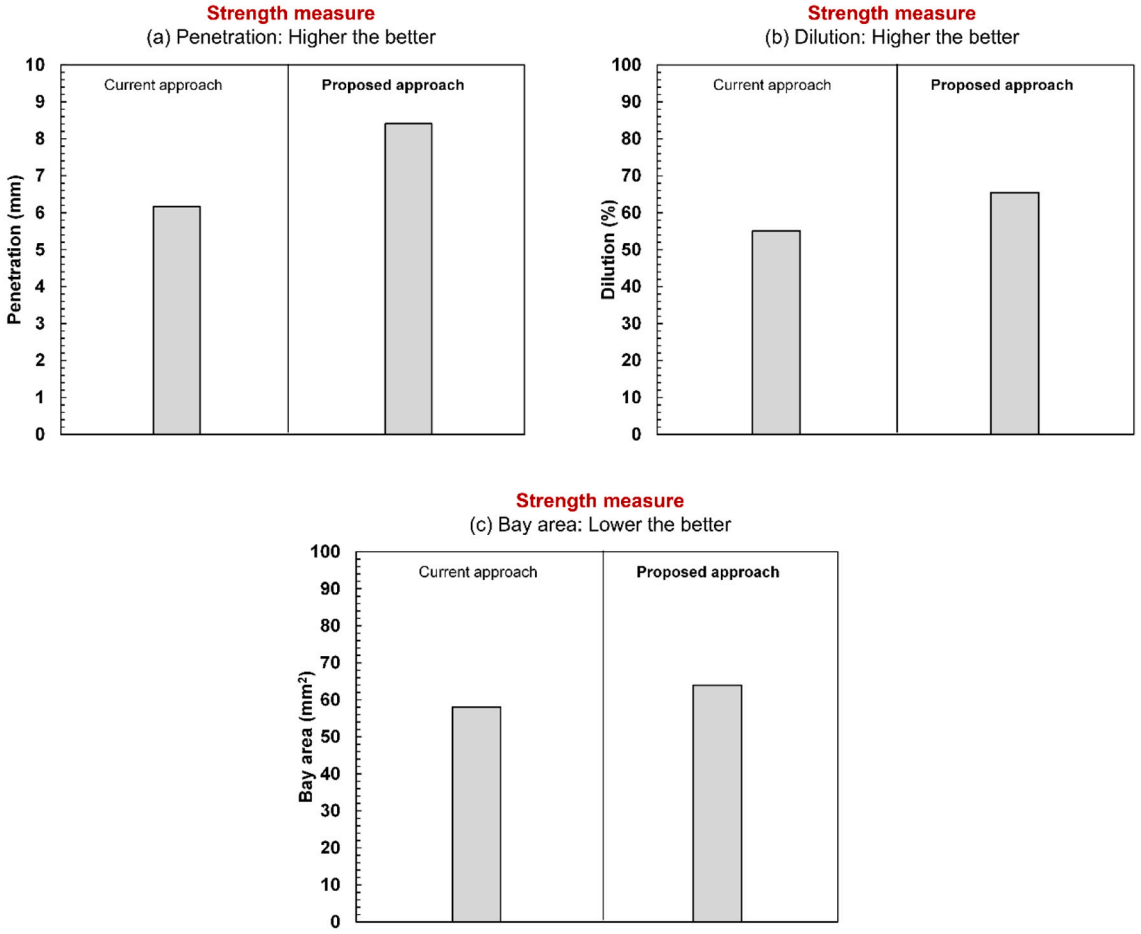

Fig. 13. Comparison of strength measures for existing and proposed process design approaches for (a) Penetration, (b) Dilution, and (c) Bay area.

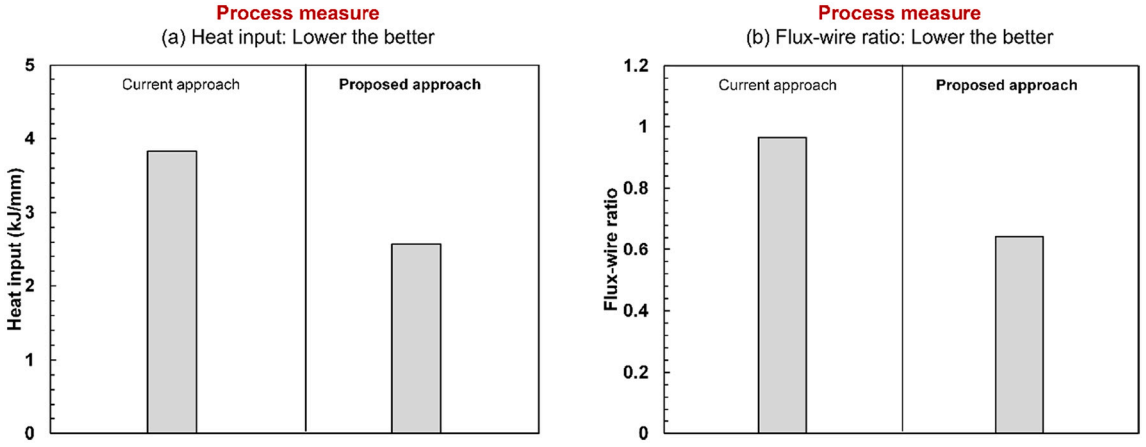

Fig. 14. Comparison of process measures for existing and proposed process design approaches for (a) Heat input, and (b) Flux-wire ratio.

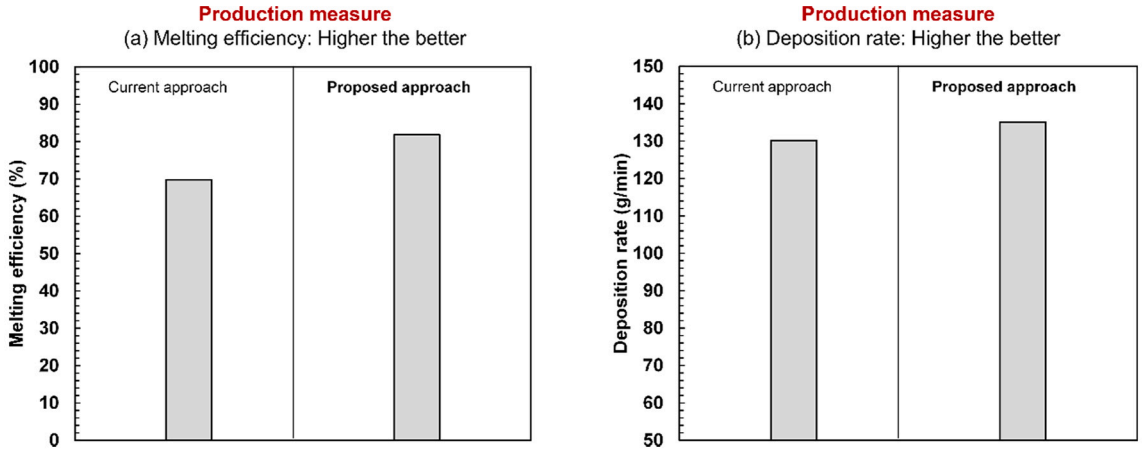

Fig. 15. Comparison of production measures for existing and proposed process design approaches for (a) Melting efficiency, and (b) Deposition rate.

to its complex nature and involved mathematical intricacies. Results presented in Fig. 12 provide critical layer thickness values that maximize the deposition rate and best utilize the process capabilities (aggregate index close to the optimal value of 0.404). The critical layer thicknesses in the test case (groove width = 14 mm), are in the ranges of 1.6–2.2 mm, 3.6–4 mm, and 4.8–5 mm.

4.3. *Efficacy of the process design*

The NGW process runs under several practical constraints that can limit productivity and efficiency, and thus there is a need to determine the optimum parameters. The process productivity for NGW in terms of the deposition rate and the aggregate index, i.e., optimum utilization of the process capabilities, for different deposition types is presented in Table 6. For deposition type 1, i.e., NGW conditions currently existing in industry for the material and flux-wire combination employed in this study (see Section 2.3), a maximum deposition rate of 130.1 g/min and an aggregate index of 0.300 were achieved. The design approach developed in this study is implemented for two deposition types; type 2 (parameters optimized to maximize deposition rate) and type 3 (parameters optimized to maximize aggregate index). There was a substantial improvement in the process capability (~35% and ~ 40% increase in aggregate index for deposition types 2 and 3, respectively) compared to the existing approach (deposition type 1). Along with the improvement in the process capability, an increase of 4% in the deposition rate for deposition type 2 is also seen.

As observed in Fig. 11, for a given layer thickness (L = 2 mm), an aggregate index of 0.404 maximizes the deposition rate. Further improvement in the utilization of the process capability, i.e., maximization of the aggregate index, comes at the cost of reduction of the deposition rate, as observed in Table 6 (deposition type 3). Maximization of the aggregate index (i.e., 0.420) led to a 9% decrease in the deposition rate compared to the deposition rate with an optimized aggregate index (deposition type 3 vs deposition type 2 in Table 6). This, however, provides additional flexibility to the end-user, as the design approach allows to alter the utilization of the process capabilities based on the desired deposition rate, making the approach application driven. Based on the results in Table 6, it can be concluded that deposition type 2 is best suited for the test case of single-pass-per-layer NGW, as it provides the maximum deposition rate with simultaneous near maximum utilization of the process capabilities. Table 6 also provides the process parameters corresponding to the three deposition types compared in this study.

The efficacy of the developed resource-efficient design approach, as seen through results presented in Table 6, can be further corroborated by findings presented in Figs. 13 to 15. The NG SAW process efficiency is primarily evaluated based on three measures, viz., strength (the attributes of the deposited weld bead), process, and production. Fig. 13(a)-(c) provide a comparison of the strength measures in terms of the bead penetration, dilution, and bay area for the design approach developed in this work and the currently used approach. Use of the developed process design approach led to a 36% increase in penetration (Fig. 13(a)), along with a 19% increase in dilution (Fig. 13(b)), as compared to the currently employed approach. Increase in these two bead attributes

influences the weld joint, with higher values signifying greater weld strengths and proper joint quality. It can be seen that there was a slight increase in the bay area (Fig. 13(c)) with the use of the proposed approach; however, it is understandable on the basis of an increase in penetration and dilution due to larger melt volume. Consequently, the notable increase of the penetration and dilution negates any detrimental effect the increase of the bay area may have on the weld strength.

The process measures, i.e., heat input and flux-wire ratio, help decide the energy and material consumption and are directly related to the cost. Lower heat input is advantageous as it reduces the negative effects like distortion and residual stress and has a positive impact on mechanical behavior. Using the developed design approach, a significant reduction of heat input (~33%) was obtained (Fig. 14(a)) without sacrificing the strength measures. Lowering heat input also helps regulate the flux-wire ratio. The flux-wire ratio provides a quantitative idea of the flux consumption and is important for the economics of the process. A lower flux-wire ratio is beneficial as it reduces flux consumption. From Fig. 14 (b), it can be seen that with the proposed approach, there was a ~ 33% decrease in the flux-wire ratio, which translates to significant savings in consumables and monetary expenses.

The two other important reflectors of productivity in NG SAW are the melting efficiency and the deposition rate. The melting efficiency is closely related to the deposition rate, as the amount of the material melted and subsequently deposited is of practical use. Higher melting efficiencies reduce material loss along with efficient utilization of the supplied heat, which directly translates to time and cost savings. With the use of the developed design approach, a ~ 17% increase in melting efficiency as compared to the currently employed approach is observed in Fig. 15(a). Increase in melting efficiency also helps to reduce the consumption of the flux, leading to further saving of the material consumables and hence the operating cost. The deposition rate is an actual industrial outcome and is an important production measure for NG SAW. As discussed earlier (see results in Table 6), for the proposed approach, there was an increase in the deposition rate (Fig. 15(b)) along with significant improvement in strength and process measures (Figs. 13 and 14).

The stated design approach is not limited to the SAW process but can be extended to other arc-welding processes. Based on the promising initial results, future work will focus on model robustness by including additional variables such as the CTWD, the height of the flux layer, voltage, electrode diameter, flux composition, and the electrode angle. The developed model will be extended for different groove widths. The identification of critical layer thicknesses for different groove widths can help in the formulation of a process map for single-pass-per-layer NGW. Based on the results of this study, it can be stated the welding current and welding speed can be the dominant parameters for the process map, however other parameters like EN ratio and flux-wire ratio (considered in this study) and those which are kept constant (CTWD, welding voltage, electrode diameter, electrode angle, flux material etc.) in this study merit further investigation.

5. Conclusions

The present investigation presents a novel design approach for the single-pass-per-layer NGW process, utilizing cost-effective and time-saving bead-on-plate experiments for the case of the AC square waveform SAW process. A new mathematical model for NGW is developed that ensures a flat top surface after deposition of each layer. The process capabilities identified through bead-on-plate experiments are coupled with the narrow gap model. The developed design approach is implemented for a test case subjected to actual production constraints and then compared with the conditions currently employed in the industry. The developed design approach positively regulates productivity by allowing end-users to bypass the resource demanding NGW experimental trials. The main conclusions drawn from this investigation are categorized and presented below.

5.1. Conclusions related to the design approach and developed model

a) The resemblance of welds in single-pass-per-layer narrow gap welding with bead-on-plate welds allows development of a process design approach for multi-layer high-thickness joints, provided each pass produces a flat surface. The mathematical model for narrow gap welding provides a necessary condition for a flat top surface, i.e., the width of the bead-on-plate weld should be >1.5 times the width of the narrow groove.
b) The bead-on-plate process model predicted deposition rate matches the experimentally achieved deposition rate in narrow gap conditions with a marginal difference of 3%. The closeness allows arriving at narrow gap welding parameters through bead-on-plate experimental data.
c) Process capability (in terms of strength, process, and production measures) identified through bead-on-plate experiments provides the feasible conditions to deposit the narrow gap welds. Within the limits of feasible weld width and reinforcement area for a given narrow gap weld design, the increment of deposition rate is possible up to a limit of process capabilities, beyond which the deposition rate drops drastically.

5.2. Conclusions related to the process parameters, and model outcome and efficacy

a) The process is more sensitive towards the change in welding current and welding speed compared to the current frequency and EN ratio.
b) The developed model provides the ability to identify the process parameters that can maximize the deposition rate whilst making best utilization of process capabilities. For the considered narrow groove design, a welding current of 665 A, welding speed of 47 cm/min, frequency of 20 Hz, and EN ratio of 0.25 maximized deposition with an optimum aggregate index of 0.404.
c) Increasing layer thickness for a given narrow groove width allows a higher deposition rate; however, the developed design approach suggests that maximum utilization of process capabilities is possible only at certain critical layer thicknesses.
d) The assessment of the developed design approach under actual production constraints reveals significant improvement in the utilization of process capabilities (~35%) combined with increased deposition rate (~4%) compared to currently employed deposition conditions in the industry.
e) The increased process capability and the deposition rate are augmented by a significant increment in resource efficiency. For a given test case, the developed design approach not only exhibited a reduction (~33%) of energy and material consumption but also improved strength measures (penetration ~36%, and dilution ~19%).

6. Outlook

The developed approach provides a pathway for selecting welding parameters based on desired layer thickness and given narrow groove width in multi-layer NGW applications, leading to optimum utilization of the process capabilities and maximization of the deposition rate. In this investigation, critical layer thickness for a given groove width is obtained, however the developed approach can be repeated to find a set of feasible layer thicknesses and groove width combinations. From a broader perspective, the developed design approach paved the way for a sustainable design for processes involving high energy and material consumption. It is necessary that contemporary and newly developed manufacturing processes like additive manufacturing continue to be assessed in the framework of resource-efficient process design.

CRediT authorship contribution statement

Uttam Kumar Mohanty: Investigation, Writing - review & editing. **Angshuman Kapil:** Investigation, Formal analysis, Visualization, Writing - original draft. **Yohei Abe:** Investigation, Resources. **Tetsuo Suga:** Resources, Funding acquisition, Project administration. **Manabu Tanaka:** Resources, Funding acquisition. **Abhay Sharma:** Conceptualization, Methodology, Funding acquisition, Supervision, Project administration, Writing - review & editing.

Declaration of Competing Interest

The authors declare that they have no known competing financial interests or personal relationships that could have influenced the work reported in this paper.

Acknowledgement

The authors acknowledge the joint research agreement between KU Leuven, Belgium, and the Joining and Welding Research Institute (JWRI), Osaka University, Japan, that supported this work. The authors would like to thank Hitachi Zosen Corporation, Osaka, Japan, for providing experimental support under Globalizing Asian Networks Project (Ja19990018). We would like to sincerely thank Mr. Takahiro Fujimoto, Dr. Mitsuyoshi Nakatani and Dr. Akikazu Kitagawa, from Technical Research Institute, Hitachi Zosen Corporation, Osaka, Japan for their detailed technical inputs during the experimental stage of the work.

Appendix A

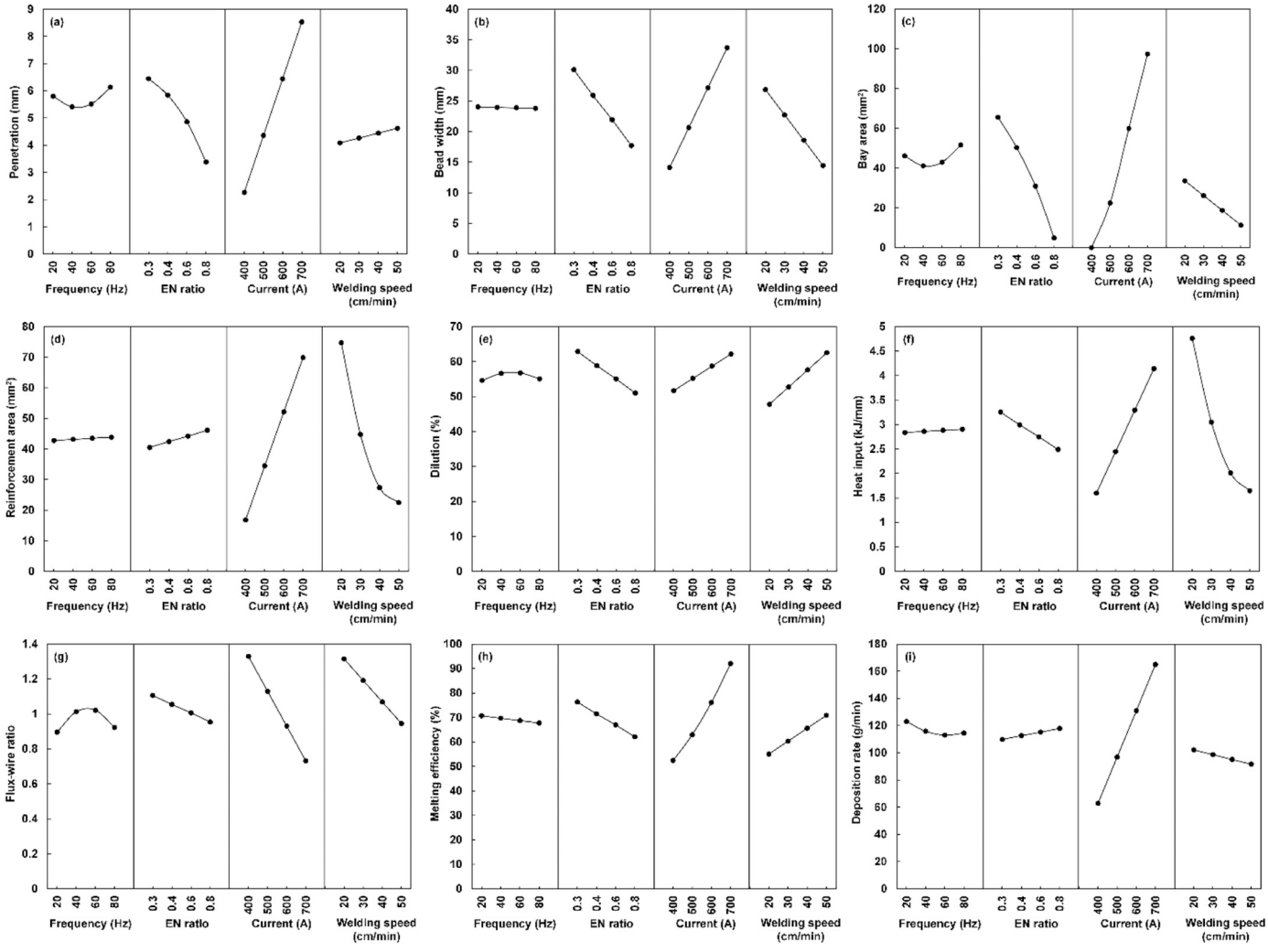

Fig. A1. Effects of welding parameters on (a) penetration, (b) bead width, (c) bay area, (d) reinforcement area, (e) % dilution, (f) heat input, (g) flux-wire ratio, (h) melting efficiency, and (i) deposition rate.

References

[1] H. Sumi, T. Kataoka, Y. Kitani, Application of narrow gap welding process with "J-STARTM welding" to shipbuilding and construction, JFE Tech. Rep. 20 (2015) 112–117.
[2] J. Norrish, Advanced Welding Processes, Springer Science & Business Media, 1992.
[3] M. Murayama, D. Oazamoto, K. Ooe, Narrow gap gas metal arc (GMA) welding technologies, JFE Tech. Rep. 20 (20) (2015) 147–153.
[4] Y. Hirai, M. Tokuhisa, I. Yamasita, K. Nisihiro, K. Akahide, T. Ukebe, Development of the narrow gap submerged arc welding process-NSA process, Kawasaki Steel Tech. Rep. 5 (5) (1982) 81–92.

[5] R. Li, T. Wang, C. Wang, F. Yan, X. Shao, X. Hu, J. Li, A study of narrow gap laser welding for thick plates using the multi-layer and multi-pass method, Opt. Laser Technol. 64 (2014) 172–183, https://doi.org/10.1016/j.optlastec.2014.04.015.
[6] S. Iwata, M. Murayama, Y. Kojima, Application of narrow gap welding process with high speed rotating arc to box column joints of heavy thick plates, JFE Tech. Rep. 14 (14) (2009) 16–21.
[7] A. Wippermann, T.G. Gutowski, B. Denkena, M.A. Dittrich, Y. Wessarges, Electrical energy and material efficiency analysis of machining, additive and hybrid manufacturing, J. Clean. Prod. 251 (2020), 119731, https://doi.org/10.1016/j.jclepro.2019.119731.
[8] T. Le-Quang, N. Faivre, F. Vakili-Farahani, K. Wasmer, Energy-efficient laser welding with beam oscillating technique–a parametric study, J. Clean. Prod. 313 (2021), 127796, https://doi.org/10.1016/j.jclepro.2021.127796.
[9] N. Goffin, L.C. Jones, J. Tyrer, J. Ouyang, P. Mativenga, E. Woolley, Mathematical modelling for energy efficiency improvement in laser welding, J. Clean. Prod. 322 (2021), 129012, https://doi.org/10.1016/j.jclepro.2021.129012.
[10] K. Venkatarao, The use of teaching-learning based optimization technique for optimizing weld bead geometry as well as power consumption in additive manufacturing, J. Clean. Prod. 279 (2021), 123891, https://doi.org/10.1016/j.jclepro.2020.123891.
[11] G. Sproesser, Y.J. Chang, A. Pittner, M. Finkbeiner, M. Rethmeier, Life cycle assessment of welding technologies for thick metal plate welds, J. Clean. Prod. 108 (2015) 46–53, https://doi.org/10.1016/j.jclepro.2015.06.121.
[12] G. Buffa, G. Ingarao, D. Campanella, R. Di Lorenzo, F. Micari, L. Fratini, An insight into the electrical energy demand of friction stir welding processes: the role of process parameters, material and machine tool architecture, Int. J. Adv. Manuf. Technol. 100 (9) (2019) 3013–3024, https://doi.org/10.1007/s00170-018-2896-7.
[13] C.F.A. Cunha, J. de Oliveira Gomes, H.M.B. de Carvalho, A new approach to reduce the carbon footprint in resistance spot welding by energy efficiency evaluation, Int. J. Adv. Manuf. Technol. 119 (9) (2022) 6503–6520, https://doi.org/10.1007/s00170-021-08472-7.
[14] A. Sharma, A fundamental study on qualitatively viable sustainable welding process maps, J. Manuf. Syst. 46 (2018) 221–230, https://doi.org/10.1016/j.jmsy.2018.01.002.
[15] G. Sproesser, A. Pittner, M. Rethmeier, Increasing performance and energy efficiency of gas metal arc welding by a high power tandem process, Procedia CIRP. 40 (2016) 642–647, https://doi.org/10.1016/j.procir.2016.01.148.
[16] Y.J. Chang, G. Sproesser, S. Neugebauer, K. Wolf, R. Scheumann, A. Pittner, M. Rethmeier, M. Finkbeiner, Environmental and social life cycle assessment of welding technologies, Procedia CIRP. 26 (2015) 293–298, https://doi.org/10.1016/j.procir.2014.07.084.
[17] K.S. Sangwan, C. Herrmann, P. Egede, V. Bhakar, J. Singer, Life cycle assessment of arc welding and gas welding processes, Procedia CIRP. 48 (2016) 62–67, https://doi.org/10.1016/j.procir.2016.03.096.
[18] A. Pittner, M. Rethmeier, Life cycle assessment of fusion welding processes—a case study of resistance spot welding versus laser beam welding, Adv. Eng. Mater. 2101343 (2022), https://doi.org/10.1002/adem.202101343.
[19] C. Favi, F. Campi, M. Germani, Comparative life cycle assessment of metal arc welding technologies by using engineering design documentation, Int. J. Life Cycle Assess. 24 (12) (2019) 2140–2472, https://doi.org/10.1007/s11367-019-01621-x.
[20] G. Sproesser, Y.J. Chang, A. Pittner, M. Finkbeiner, M. Rethmeier, Sustainable technologies for thick metal plate welding, in: R. Stark, G. Seliger, J. Bonvoisin (Eds.), Sustainable Manufacturing, Springer, Cham, 2017, pp. 71–84, https://doi.org/10.1007/978-3-319-48514-0.
[21] T. Manzoli, E. Caccia, Narrow gap welding of heavy gauge steel nuclear components, Weld. Int. 3 (5) (1989) 417–423, https://doi.org/10.1080/09507118909447675.
[22] P.T. Houldcroft, Submerged-Arc Welding, Woodhead Publishing, 1990.
[23] P. Layus, P. Kah, V. Gezha, Advanced submerged arc welding processes for Arctic structures and ice-going vessels, Proc. Inst. Mech. Eng. B J. Eng. Manuf. 232 (1) (2018) 114–127, https://doi.org/10.1177/0954405416636037.
[24] I. Sejima, T. Godai, M. Kawahara, H. Nomura, Developments and Applications of Narrow Gap Welding Processes in Japan, International Institute of Welding, Portugal, 1981.
[25] F. Fusari, P. Marangoni, M. Musti, S. Alberini, Improvements in the welding technology for heavy wall pressure vessels 2 ¼ Cr 1Mo ¼ V low alloy steels, in: Pressure Vessels and Piping Conference vol. 57984, American Society of Mechanical Engineers, 2017 p. V005T05A012.
[26] A. Ando, K. Kobayahi, T. Iijima, A study of tandem SAW methods using current waveform control, in: Abstracts of the Japan Welding Society National Conference 86, 2010, pp. 146–147.
[27] M. Tokuhisa, Y. Hirai, N. Nishiyama, I. Yamashita, K. Nisho, K. Nakatsuji, Development of High-Quality Narrow Gap Submerged Arc Welding Consumables for Cr-Mo Steel, Kawasaki Steel Tech. Rep 15, 1986, pp. 74–83.
[28] Y. Abe, T. Fujimoto, M. Nakatani, M. Shigeta, M. Tanaka, Study on proper welding condition for ultranarrow gap submerged arc welding, Weld. Int. 35 (7–9) (2021) 369–381, https://doi.org/10.1080/09507116.2021.1980298.
[29] S. Alfaro, Mathematical Modelling in Narrow Gap Submerged Arc Welding, PhD thesis, Cranfield Institute of Technology, 1989.
[30] S.C. Alfaro, R.L. Apps, Mathematical modelling of narrow gap submerged arc welding, in: 8th International Conference, Offshore Mechanics & Arctic Eng 3, 1989, pp. 469–473.
[31] Y. Abe, T. Fujimoto, M. Nakatani, M. Shigeta, M. Tanaka, Development of a welding condition optimization program for narrow gap SAW, Q. J. Jpn. Weld. Soc. 38 (2) (2020) 98s–102s.
[32] U.K. Mohanty, Y. Abe, T. Fujimoto, M. Nakatani, A. Kitagawa, M. Tanaka, T. Suga, A. Sharma, Performance evaluation of alternating current square waveform submerged arc welding as a candidate for fabrication of thick welds in 2.25Cr-1Mo heat-resistant steel, J. Press. Vessel. Technol. 142 (4) (2020), 041506, https://doi.org/10.1115/1.4046785.
[33] R.E. Toma, S.D. Brandi, A.C. Souza, Z. Morais, Comparison between DC (+) and square wave AC SAW current outputs to weld AISI 304 for low-temperature applications, Weld. J. 90 (9) (2011) 153s–160s.
[34] U.K. Mohanty, A. Sharma, Recent developments in AC square waveform welding, Mater. Today Proc. 45 (2021) 5709–5713, https://doi.org/10.1016/j.matpr.2021.02.516.
[35] J. Pepin, Effects of Submerged Arc Weld (SAW) Parameters on Bead Geometry and Notch-Toughness for X70 and X80 Linepipe Steels, Dissertation, University of Alberta, 2009, https://doi.org/10.7939/R3N061.
[36] U.K. Mohanty, A. Sharma, M. Nakatani, A. Kitagawa, M. Tanaka, T. Suga, A semi-analytical nonlinear regression approach for weld profile prediction: a case of alternating current square waveform submerged arc welding of heat resistant steel, J. Manuf. Sci. Eng. Trans. ASME 140 (11) (2018), 111013, https://doi.org/10.1115/1.4040983.
[37] F.C. Campbell, Joining: understanding the basics, ASM Int. (2011) 1–323.
[38] R.S. Chandel, Electrode melting and plate melting efficiencies of submerged arc welding and gas metal arc welding, Mater. Sci. Technol. 6 (8) (1990) 772–777, https://doi.org/10.1179/mst.1990.6.8.772.
[39] A. Sharma, N. Arora, B.K. Mishra, Statistical modeling of deposition rate in twin-wire submerged arc welding, Proc. Inst. Mech. Eng. B J. Eng. Manuf. 223 (7) (2009) 851–863, https://doi.org/10.1243/09544054JEM1342.
[40] P.K. Swamee, A. Tyagi, Describing water quality with aggregate index, J. Environ. Eng. 126 (5) (2000) 451–455, https://doi.org/10.1061/(ASCE)0733-9372(2000)126:5(451).